Available online at www.sciencedirect.com
ScienceDirect
Journal of the European Ceramic Society 27 (2007) 3277–3285
www.elsevier.com/locate/jeurceramsoc

Liquid metal/ceramic interactions in the (Cu, Ag, Au)/ZrB_2 systems

Alberto Passerone [a,*], Maria Luigia Muolo [a], Rada Novakovic [a], Daniele Passerone [b]

[a] *IENI-GE, CNR, Via De Marini 6, 16149-Genoa (I), Italy*
[b] *Empa-Mater. Sci. & Techn., Überlandstrasse 129, CH-8600 Dübendorf, Zurich (CH), Switzerland*

Received 16 September 2006; received in revised form 7 December 2006; accepted 16 December 2006
Available online 8 March 2007

Abstract

Wetting and spreading experiments on ZrB_2 in contact with liquid Cu, Ag and Au have been performed by the sessile drop technique under a vacuum. The wetting and spreading characteristics and the interfacial reactions are discussed as a function of time and of the metal involved. The interfacial morphologies, analysed by optical microscopy, SEM and EDS show the presence of regular interfaces without macroscopic reaction layers. Gold, to a very large extent and copper are shown to give rise to extensive penetration along grain-boundaries, whereas silver neither wets nor penetrates. Interfacial diffusion/dissolution is taken into account and the consequent changes in liquid metal surface tension and wetting behaviours have been evaluated by means of thermodynamic calculations.

Moreover, interfacial energetics at the atomistic level has been investigated by means of pseudopotential-based Density Functional Theory (DFT) technique. It is shown how the calculation of the *ideal work of separation* on the specific transition metal borides-molten metal systems can be used to interpret the wetting behaviour. Moreover, the dependence of the adhesion behaviour on the electronic structure at the interface and on the interface epitaxy and composition is also briefly discussed.

Keywords: A. Joining; B. Interfaces; C. Wettability; D. Borides

1. Introduction

Zirconium diboride is a member of a family of materials – the transition metal diborides – with extremely high melting temperatures, high thermal and electrical conductivity, excellent thermal shock resistance, high hardness and chemical inertness. These materials, also referred to as Ultra High Temperature Ceramics (UHTC's), constitute a class of promising materials for use in aggressive environments, where, for example high temperatures and high thermal fluxes are involved.[1]

Often, to exploit the peculiar characteristics of these ceramic materials the necessity arises to join the ceramic parts one to the other or to special metallic alloys by means of diffusion bonding or brazing techniques. In the last case, as the behaviour of a metal–ceramic joint is ruled by the chemical and the physical properties of the interface, the knowledge of the interfacial energetics, i.e. of interfacial tensions, interfacial reactions and wettability is mandatory.

Many efforts have been made to improve wetting in metal–ceramic systems.[2] Two ways are widely used: one is to modify the ceramic surface by some specific coatings, in order to let the braze metals spread on this new surface, the other one is to add reactive elements to the braze which can form intermediate products at the interface more readily wetted by the liquid alloy. For example, the addition of Ti to Ag or Cu alloys involves the formation of Ti compounds (TiO_x, TiC or TiN on oxides, carbides and nitrides, respectively[3–5]) at the metal–ceramic interface which, due to their more "metallic" character, are wetted better than the underlying ceramic. Active metal additions can also act through an adsorption process, where the additional element accumulates at the solid–liquid interface lowering the interfacial energy and, as a consequence, the contact angle affecting also the spreading kinetics.[6–8]

In the past years the wetting experiments performed on ZrB_2 are quite scarce and from them it is difficult to derive general rules (Table 1). As in the case of nearly all ceramic materials, the reasons for this can be attributed to different factors. First of all, the chemical composition and the surface structure of the solid specimens are hardly specified. Indeed, these materials are obtained by various sintering techniques.

* Corresponding author.
E-mail address: a.passerone@ge.ieni.cnr.it (A. Passerone).

0955-2219/$ – see front matter © 2007 Elsevier Ltd. All rights reserved.
doi:10.1016/j.jeurceramsoc.2006.12.008

Table 1
Wettability data obtained in past years (literature values)

Boride	Metal	Contact angle	Temperature (K)	Medium
ZrB_2[25]	Fe	55	1823	Vacuum
ZrB_2[25]	Co	39	1773	Vacuum
ZrB_2[25]	Ni	42	1773	Vacuum
ZrB_2[26]	Ag	114	1373	He
ZrB_2[26]	Ag	70	1873	He
ZrB_2[27]	Ga	127	1073	Vacuum
ZrB_2[27]	In	114	573–773	Ar
ZrB_2[27]	Al	106–160	1173–1523	Vacuum
ZrB_2[27]	Ge	102	1273	Ar
ZrB_2[27]	Sn	101	523–873	Ar

Even if innovative sintering procedures are used[9–15] high densification can hardly be obtained, and the final microstructure is coarse and an amount of residual porosity is present, because the matter transfer active at the sintering temperature ($T > 1700$ K) takes place through evaporation/condensation rather than volume diffusion processes. One important consequence is that the surface porosity enhances the surface roughness to values which may lead to contact angles not representing the "real" metal/ceramic interface (it should be remembered that a roughness $R \ll 0.1$ μm should always be used[16] to obtain reliable contact angle values). On the other hand, sintering aids used to reach nearly theoretical densities, not only modify the ceramic structure, but can also form new phases, grain-boundary precipitates and new solid solutions: in all cases they change the nature of the ceramic body and that of the molten phase, so that the contact angle measurements should be referred to the new system, which is often difficult both to characterize or to reproduce[17].

Moreover, in wetting experiments a third "component" besides the solid and the liquid phases plays a major role: the surrounding atmosphere. Indeed, one of the most common sources of scatter among reported contact angle data comes from the contamination of the liquid phase by active gases like oxygen. Oxygen transport phenomena related to the modification of liquid surface tension, solid–liquid interfacial tension and contact angles have been thoroughly studied in recent years.[18–24] One of the most important results is that, on top of the classical thermodynamic approach, dynamic transport processes must be taken into account, which show how, in many cases, the combined effects of metal atoms and sub-oxides evaporation can allow experiments to be carried out in "clean" conditions of the liquid metal surface even if equilibrium thermodynamics should foresee metal oxidation.[18] On the other hand, once they reach the liquid surface, active gases diffuse through the liquid phase and can reach the solid–liquid interface modifying its energetics by adsorption and/or formation of new phases.

This paper reports the results of wetting, spreading and penetration of "pure" zirconium boride ZrB_2 ceramics by Cu, Ag and Au chosen as "non-reactive" metals to study the intrinsic characteristics of the diboride.

The results will be discussed in terms of interfacial thermodynamic properties (work of adhesion, interfacial tension) and interfacial microstructures. The variation of surface tension under the effects of diffusing elements will be taken into consideration through thermodynamic models.

2. Materials and wetting experiments

The sintered ceramic bodies have been prepared by ISTEC-CNR[15] starting from pure ZrB_2 powders (H.C. Stark, Grade B, Germany), while pure Cu, Ag and Au (Marz grade 99.998) have been used, in the form of small, pre-melted drops of 0.5–1 g weight. The ceramic surface, carefully polished, was pre-treated at 1350 K under a vacuum in the presence of a Zr getter.

Wetting experiments have been performed by the Sessile-Drop technique[28,29] in a special tubular furnace made up of two concentric, horizontal, alumina tubes, connected to a high vacuum line. Between the tubes an Ar flow is maintained, to avoid any diffusion of atmospheric oxygen into the working chamber at high temperature. A vacuum better than 10^{-4} Pa or a controlled atmosphere can be set in the working tube, the oxygen partial pressure being measured by a solid state gauge at the exit of the inner tube. An optical line allows sessile drops in the centre of the working chamber to be imaged by a CCD camera. A specifically developed image analysis software (ASTRAView©[30,31]) allows the surface tension, contact angles and other drop's parameters to be computed in real time during the experiments.

All sessile drop experiments reported here have been performed at $T = 1.05T_m$ in order to obtain results at the same reduced temperature. The ceramic plates (15 mm × 15 mm × 2 mm) and the metal pieces were put in the centre of the tube when all the physico-chemical parameters were at equilibrium. The samples, maintained at temperature for about 1 h, were cooled down quickly, by pulling them out of the furnace.

A Zr getter has been put around the sample in order to reduce its oxidation. Taking into account the oxygen partial pressure coming from the oxidation of the Zr getter we can estimate an equilibrium (limiting) $P(O_2)$ of the order of 10^{-27} Pa.

After polishing, the average surface roughness of the ceramics, was found to be in the order of 0.05 μm. Contact angles are measured with a reproducibility of ±3° between the runs. However, the presence of a certain surface porosity can lead to occasional higher uncertainties in the measured contact angles, especially when θ is greater than 130° or smaller than 30°.

The specimens have been characterized by optical and SEM observations and EDS analysis.

3. Results

3.1. Wetting

Wetting results are reported in Fig. 1(a and b).

The analysis of the wetting kinetics shows that, surprisingly enough, Cu, Ag and Au behave in a different way. While the "initial" contact angles (i.e. the contact angle which can be measured after the drop has melted) are of the same order of magnitude (≫100° in the order Ag > Cu > Au), a spreading kinetics

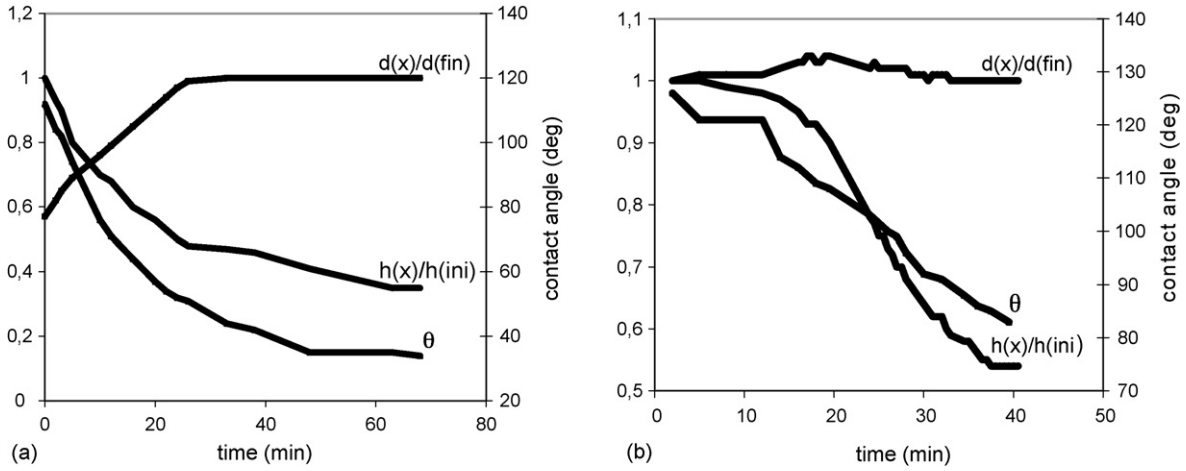

Fig. 1. Spreading kinetics on ZrB_2 at $T = 1.05T_m$. Contact angle (right scale), normalized height (h) and diameter (d) (left scale); $h(x)$, $d(x)$: current values; h(ini), d(fin): initial and final values. (a) Au/ZrB_2 and (b) Cu/ZrB_2.

takes place for Cu and Au, leading to an "apparent" final contact angle of 80° and 35°, respectively. At variance, the Ag contact angle ($\theta \approx 130°$) remains practically unchanged with time. It can be added that, in one particular experiment, after 30 min the temperature was raised up to 1550 K: the only visible effect was a remarkable thinning of the Ag drop due to evaporation.

However, when analysing jointly the data relative to the height and diameter variations some peculiar effects appear. As shown in Fig. 1(a), the gold drop base diameter increases during the first 25 min, with a parallel decrease in contact angle and drop height. After this period the base diameter keeps constant while both the drop height and contact angle decrease steadily. This effect is due to the presence of bulk porosity in the sintered borides: a part of the liquid mass flows inside the ceramic body, so that the evolution of both drop height and contact angle can be interpreted as due to a volume variation with (nearly) constant base diameter. This effect, i.e. the dependence of contact angles on purely geometrical parameters as a consequence of volume shrinkage, becomes the most relevant process after the contact angle has reached the value of about 50° for Au and between 100° and 110° for Cu. Micrographic examination shows a large penetration of gold along the grain boundaries, filling up all the empty spaces inside the ceramic. The same effect is found in the case of copper drops, even to a lesser extent. For these reasons, it is not possible to assign the final contact angles as "intrinsic" contact angles, because the volume variation and the pinning of the triple line (constant diameter) are the main causes of the contact angle decrease. However, it is equally clear that gold and copper wet the ceramic boride much better than silver, giving equilibrium contact angles of the order of less than 50° for Au and about 100° for Cu. These limiting values are deduced from the contact angle values measured before any grain boundary penetration has taken place, at least on the macroscopic scale. Further confirmation of this result is found when measuring the contact angles of micro-drops on single boride grains, as shown in Fig. 2.

These results are interesting "per se", and should be discussed in terms of possible interactions at the solid–liquid interface. Indeed, a significant change in contact angle can be attributed to

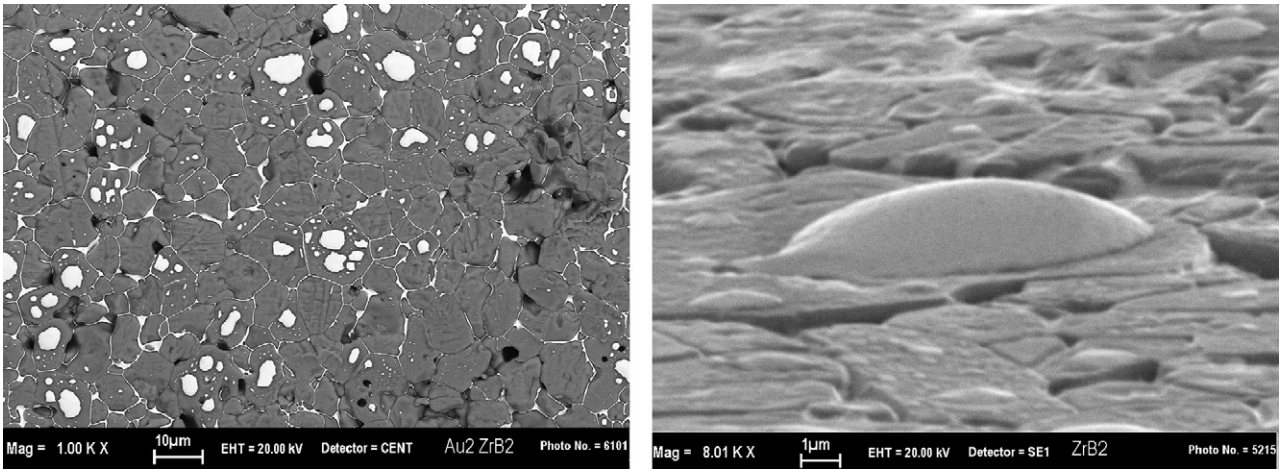

Fig. 2. Gold microdrops sitting on single ZrB_2 grains at the ceramic surface.

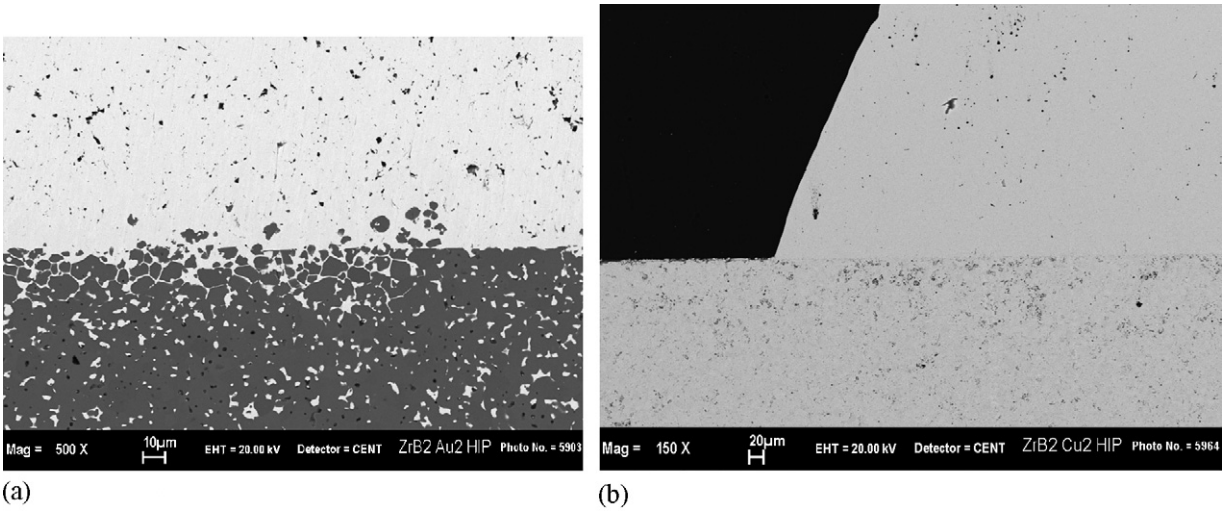

Fig. 3. (a) Au–ZrB_2 interface and (b) Cu–ZrB_2 interface.

two possible causes, both related to dissolution/reaction at the solid–liquid interface, namely:

(1) Variation of the liquid surface tension due to Zr and/or B dissolution.
(2) Re-adsorption of Zr at the solid–liquid interface, with Zr playing its well known role[2,29] of "active" metal in brazing processes.

To clarify the relative weight of these two hypotheses, a special attention was paid to the evaluation of the influence of Zr and B on the surface tension of liquid (Cu, Ag, Au) and on the enthalpy of mixing of Zr into the same liquid metals through thermodynamic models.

These points are addressed in Sections 4.1 and 4.2. Moreover, in order to build the necessary models on experimental data, the interfacial microstructures (Section 3.2) of the solidified drops have been examined.

3.2. Interface characterization

The microstructure of the solid–liquid interfaces have been studied on vertical sections by SEM and EDS microanalysis. All the metallographic sections show a very sharp interface where grains are very often stripped away into the liquid phase (Fig. 3). This is particularly evident in the case of Au samples, whereas with Cu this phenomenon is less pronounced and nearly absent in the case of Ag.

In Au–ZrB_2 specimens, ZrB_2 grains are found both at the drop surface and inside the metallic phase, with a well developed crystalline structure (Fig. 4). In this case, the grains dimensions are similar to those of the grains forming the sintered solid. As already mentioned, complete grain boundary penetration occurred in the Au samples and to a lesser extent in the Cu samples too. Fig. 5 clearly shows this phenomenon, with the gold phase embedding the boride grains at the ceramic free surface. The same phenomenon is found inside nearly all the ceramic phase thickness (Fig. 3).

4. Modelling

As mentioned in previous paragraphs, the dynamic evolution of contact angles in Cu and Au systems calls for the presence

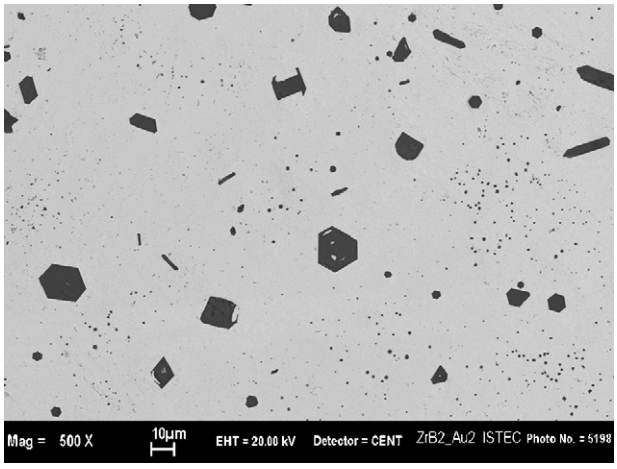

Fig. 4. Zirconium boride crystals inside the Au molten matrix.

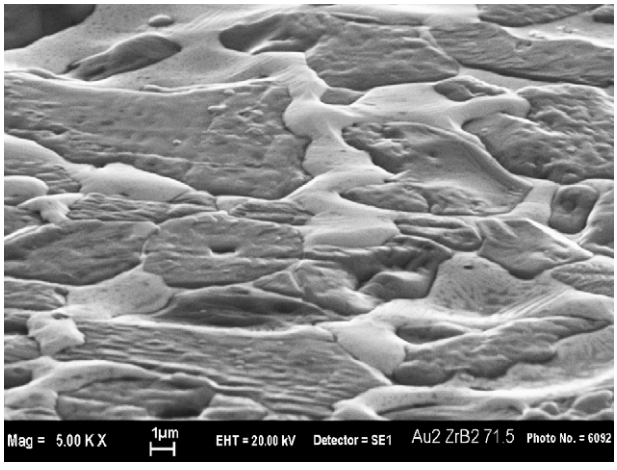

Fig. 5. Au penetration along grain boundaries at the surface.

of interfacial interactions which should lead to diffusion of elements of the ceramic phase into the molten liquid metal. In order to evaluate more quantitatively these effects, data are needed on the enthalpy of mixing and on the effects of Zr and B on the liquid surface tension. To this end, due the paucity of reference data, thermodynamic calculations have been made, which are presented in the following paragraphs. Moreover, specific calculations have been performed in the framework of plane wave density functional theory (DFT), to understand the intrinsic nature of the bonding at the interfaces between ZrB_2 and the transition metals Ag, Au and Cu and to get an independent validation of the results experimentally determined.

4.1. Surface tension

The thermodynamic data on the Au–B and Cu–B systems as well as their phase diagrams are still incomplete,[32] while the phase diagram of the Ag–B system is even not yet assessed. The Cu–B phase diagram shows the existence of a simple eutectic.

The assessment of Au–B phase diagram of a monotectic type indicates higher uncertainties in respect to the Cu–B. The enthalpy of mixing data of Cu–B liquid alloys together with the estimated excess entropy of mixing, S_M^{xs}, [33] were combined using the standard thermodynamic relations to calculate the excess Gibbs energy term, G_M^{xs} and Gibbs energy of mixing, G_M. The enthalpy of mixing of Cu–B liquid alloys[34] indicate positive deviation of their thermodynamic properties from the Raoult's law, and thus the related thermophysical properties deviate negatively from the corresponding ideal values (Fig. 6); in particular, for the surface tension and viscosity, a complete lack of experimental data is evident.

Although the Quasi Chemical Approximation (QCA)[35] was basically formulated for a metal–metal alloy, it has also been applied to study the mixing behaviour of metal–metalloid systems such as the Cu–Si and the Ni–Si,[36] suggesting some limitations to the QCA formulations. Taking into account that

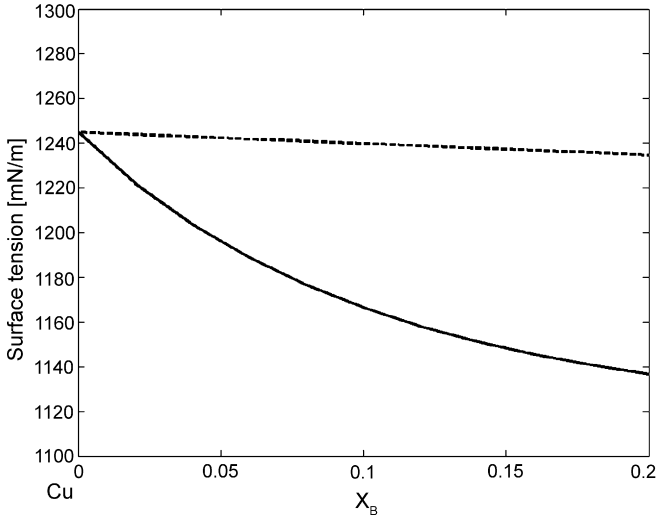

Fig. 6. Surface tension isotherm of Cu–B liquid alloys calculated by the QCA at $T = 1870$ K (the dashed line represents the values calculated by the ideal solution model).

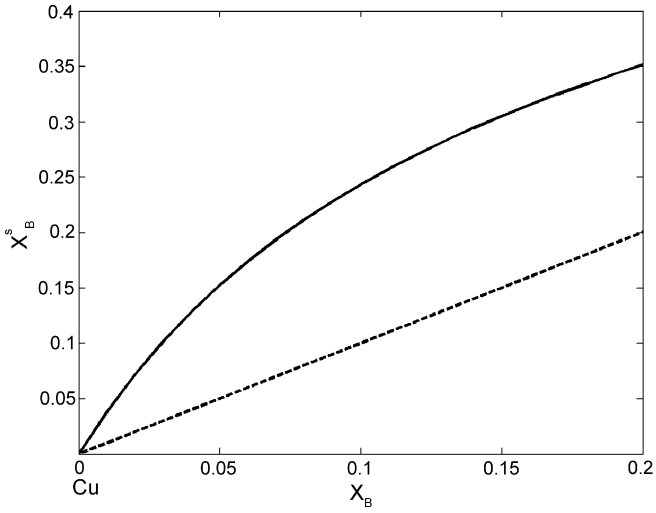

Fig. 7. Surface composition (X_B^s) vs. bulk composition (X_B) for Cu–B liquid alloys at $T = 1870$ K calculated by the QCA (the dashed line represents the values calculated by the additive rule).

the static structure factors of these alloys differ from those of a metal–metal system, the QCA for regular solution can be applied at least as a first approximation to calculate the surface properties of a metal–metalloid system. Due to the close similarity of B with Si,[37] the surface properties of Cu–B liquid alloys have been also analysed in the framework of the QCA. The surface tension and the surface composition of Cu–B liquid alloys have been calculated up to 20 at.% B at $T = 1870$ K. The surface tension isotherm of Cu–B liquid alloys (Fig. 6) exhibits a tensioactive effect of boron over this concentration range. As a consequence, B-atoms segregate to the surface at all bulk concentrations (Fig. 7).

These results, obtained at 1870 K because all input data for calculations are referred to this temperature, can be qualitatively extrapolated to the experimental temperature ($T = 1.05T_m$). This means that boron dissolution ($X_B \ll 0.1$) can cause a lowering of the order of a few percent in the liquid metals surface tension. This effect promotes the wetting process, but cannot be taken as the most important mechanism (see Table 3, where the W_{adh} is corrected by a hypothetical 5% reduction).

4.2. Enthalpy of mixing

The activities and the enthalpy of mixing of Ag–Zr,[38] Au–Zr[38,39] and Cu–Zr[40–43] molten alloys deviate negatively from the ideal values, and according to this, the three alloy systems belong to the class of liquid alloys that exhibits a tendency towards compound formation.[35] As a consequence, the related thermophysical properties deviate positively from the corresponding ideal values.[44,45]

The scarce enthalpy of mixing data on Ag–Zr[38] and Au–Zr[38,39] liquid alloys measured at $T = 1473$ K as well as a more complete enthalpy data set on the Cu–Zr system[42,41,40] measured at temperatures ranging between 1468 and 1499 K are shown in Fig. 8. These results can be compared with those derived by the Miedema's model[52] (Table 3): they are in the same range and in the same order, even if this last model yields

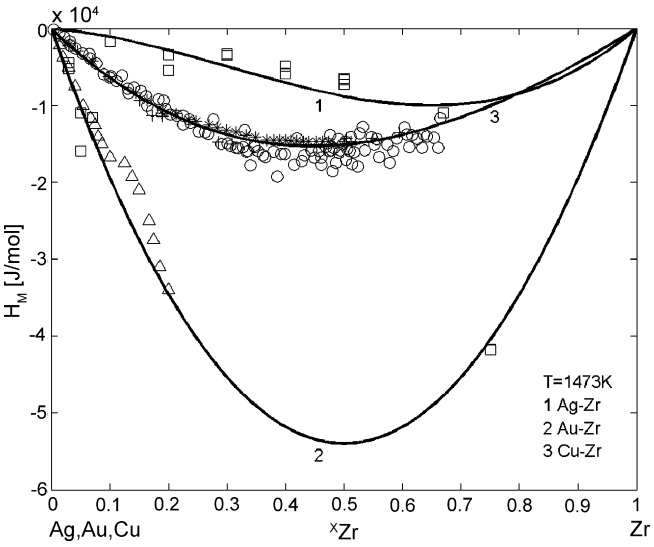

Fig. 8. The enthalpy of mixing for molten X–Zr (X = Ag, Au, Cu) alloys calculated by the QCA at T = 1473 K together with experimental data on H_M measured at T = 1473 K (□ ,[38] + ,[40] △ [39]), T = 1499 K (*[42]) and T = 1468–1485 K (◯[41]), respectively.

higher values, as discussed by several authors. It can be seen that among the systems mentioned above, the most interacting is the Au–Zr, followed by the Cu–Zr and Ag–Zr. The dissolution of Zr into molten Au, Cu and Ag, respectively, can be estimated by the partial enthalpy of mixing of Zr. In particular, the partial enthalpy at infinite dilution $\Delta\bar{H}_M$ indicates the driving force for Zr-dissolution in Au, Cu and Ag, respectively.

No data are available for the enthalpy of mixing of boron in molten Ag and Au, while estimations can be found for the Cu–B system.[34] The formation of Cu–B alloys takes place with an endothermic effect, so that it is likely that the $\Delta\bar{H}_M$ is small and positive, indicating a low driving force for mixing. On a qualitative basis, similar effects are expected also for the Ag–B and Au–B systems.

Based on the Mendeleev's rule, the enthalpy and entropy of a certain system may be estimated by comparison with similar systems according to the position of their constituents in the Periodic Table.[46] In view of this rule, the mixing behaviour of Ag–B and Au–B liquid alloys should be similar to that of the Cu–B.

4.3. DFT modelling

To understand the nature of the bonding at the interfaces between ZrB_2 and the transition metals Cu, Ag and Au, a first-principles study has been done.

In the case of Ag and Au, the hypothesis of a (1 1 1) interface of metal parallel to a Zr- or B-terminated layer of boride gives rise to a mismatch in the lattice parameters of about 10%, whereas for copper/zirconium diboride a mismatch of about 20% has been found. Thus, the calculations have been made only for the Ag and Au cases.

The interfaces are considered as "solid–solid". In this way the work of separation is obtained, which is the reversible work needed for separating the interface into two free surfaces, with the implicit assumption that plastic and diffusional degrees of freedom are suppressed.

Though this severe approximation, this quantity gives a useful indication about the mechanical strength of the interface.[47]

The calculations were performed in the framework of plane wave density functional theory, using the "Espresso" package[48] and the Perdew-Burke-Ernzerhof (PBE) generalized gradient approximation.

To model the interface, periodically repeated supercells with 4 or 5 layers of metal and 4.5 cells for ZrB_2 have been used examining separately the interface of the metal with a Zr-terminated slab and a B-terminated slab. Each layer is composed of 4 (Zr, Ag/Au) or 8 (B) atoms.

The lattice parameters of ZrB_2 are kept like in unstrained bulk. The *in-plane* lattice constant of the metal phase is adjusted to give a commensurate structure with the ZrB_2 slab. The metal *out-of-plane* lattice constant is optimized in bulk calculations to minimize the bulk strain introduced by the *in-plane* lattice distortion.

"Ultrasoft" pseudopotentials have been used to describe electron–core interactions for Au, Ag, Zr and B with non-linear core corrections.

Valence states include 5p, 5s and 4d for Ag, 5d, 6s and 6p for Au, 4s, 4p, 4d, 5s and 5p for Zr and 2s and 2p shells for B. The pseudopotential for Au includes scalar relativistic effects.

The smooth part of the wave functions is expanded in plane waves with a kinetic energy cutoff of 25 Ry, whereas the cutoff or the augmented electron density is 100 Ry (1 Rydberg = 13.6 eV).

To ensure a converged interfacial energy, the k-sampling of the surface Brillouin zone included 4k-points (k points are necessary because the simulation cell is small). We plan to increase this value for improving convergence.

The pseudopotentials have been tested for the bulk lattice constant obtaining satisfactory results for all species. All calculations are performed by relaxing the position of all atoms until residual forces are less than 0.03 eV Å^{-1} (0.5 pN).

The first value we extract from our calculations is the work of separation, defined as[49]:

$$W_{sep} = \frac{E_{sl1} + E_{sl2} - E_{int}}{2A},$$

where E_{int} is the total energy of the supercell with the interface system, E_{sl1} and E_{sl2} the total energies of the same supercell, when one of the slabs is kept and the other one is replaced by vacuum and A is the interface area within one supercell (there are two identical interfaces/supercell).

Preliminary values of the work of separation are reported in Table 2 (all results with 4k-points).

These results indicate that the interface between Au and ZrB_2 (with Zr termination) is energetically more stable than

Table 2
Work of separation (J/m^2)

	Ag	Au
B terminated surface	2.03	2.09
Zr terminated surface	2.47	3.725

Table 3
Thermodynamic and experimental data for (Ag, Cu, Au)/ZrB_2 systems

System	$\Delta\bar{H}_M$ (kJ/mol)	$\Delta\bar{H}_M$ (kJ/mol) Miedema[52]	Contact angle (°)	γ_{lv} (J/m^2)		W_{adh} (J/m^2)		$\gamma_{lv}\cos\theta$ (J/m^2)	
Ag/ZrB_2	−6	−87	∼150	915[a]		∼100		−790	
Cu/ZrB_2	−74	−116	80	1.272[a]	1.208[b]	1.493[a]	1.418[b]	0.220[a]	0.210[b]
Au/ZrB_2	−216	−303	51	1.095[a]	1.040[b]	1.748[a]	1.695[b]	1.100[a]	0.655[b]

$\Delta\bar{H}_M$ at $T = 1473$ K, contact angle and γ_{lv} at $T = 1.05\ T_m$; $\Delta\bar{H}_M$ values are referred to the dissolution of Zr into the molten metal (Ag, Cu, Au).
[a] Pure metal.
[b] In the presence of boron ($X_B = 0.1$).

that involving silver. We underline that this kind of calculation provides information about the *energy part* of the free energy (at $T = 0$ K), neglecting entropic contributions that are of course present at higher temperatures.

Nevertheless, although the behaviour of W_{sep} can give only qualitative indications about the work of adhesion, this trend seems confirmed by the results summarized in Table 3.

In order to understand why the Au/Zr interface is more energetically favourable than the others, two additional kinds of analysis have been made.

The first one concerns the behaviour of the electronic density across the interface, in the two extreme cases of the Au/Zr and Au/B interfaces. The results are shown in Figs. 9 and 10.

To get an idea of the density scale for covalent bonding, one can observe charge density isosurfaces at different levels. In Fig. 9, the isosurface for 0.09 electrons/(a.u.)^3 is shown (this value corresponds to a good visual description of the well known covalent bonding between boron atoms). At this value, no covalent bonding appears at the interface. For comparison, in the Fe–C case at metallic ceramic interfaces[50] the charge density in the middle of the bond is 0.12 electrons/(a.u.)^3.

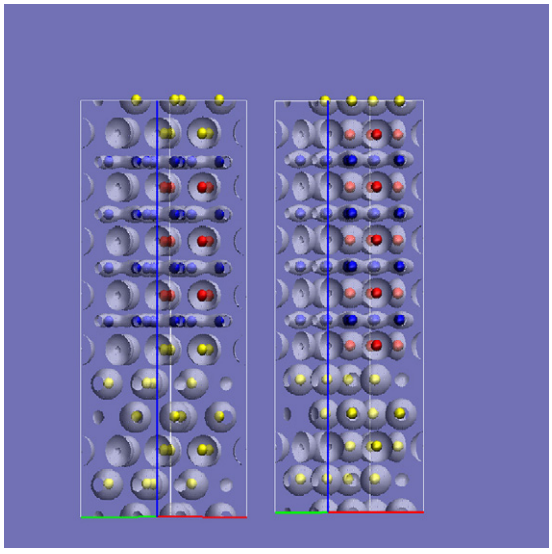

Fig. 9. B-terminated (left) and Zr-terminated (right) Au/ZrB_2 interface at the equilibrium geometry obtained from a DFT plane wave calculation. The isosurface of electronic density at the 0.09 electron/(a.u.)^3 is highlighted. One can note that for this isosurface the electronic density concentrates around the nuclei for the Au (yellow) and Zr (red) atoms, whereas for B (blue) atoms the in-plane directional, covalent bonding is elucidated. (For interpretation of the references to colour in this figure legend, the reader is referred to the web version of the article.)

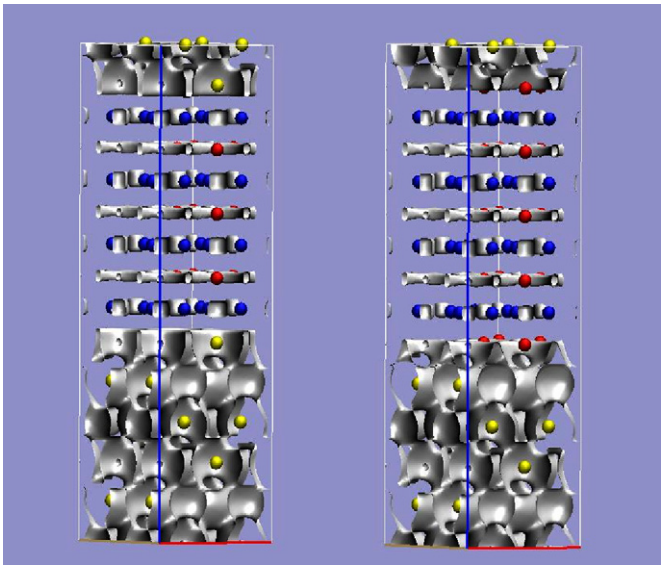

Fig. 10. B-terminated (left) and Zr-terminated (right) Au/ZrB_2 interface at the equilibrium geometry obtained from a DFT plane wave calculation. The isosurface of electronic density at the 0.03 electron/(a.u.)^3 is highlighted. One can note that for this isosurface the electronic density describes the metallic bonding in gold (yellow). This metallic bonding extends to the interface in the Zr-terminated (red) case on the right, whereas it leaves a gap in the B-terminated (blue) case shown on the left. (For interpretation of the references to colour in this figure legend, the reader is referred to the web version of the article.)

Decreasing the isosurface value to 0.03 electrons/(a.u.)^3 no covalent bonding is present again at the B-terminated interface. However, inspection of the Au section shows that this value for the isosurface describes the metallic bonding within the metal. At the interface to the Zr-terminated ZrB_2 section this metallic electronic distribution appears to penetrate down to the level of the zirconium layer, indicating, in this case, the possibility of a metallic bonding at the interface.

Talking about related studies, de la Mora, et al.[51] studied different bulk MeB_2 compounds with Me = Mg, Al, Zr, Nb, Ta, using DFT. They look at charge density and conductivity, in plane and along z. They found that the B–B bonds are highly covalent (directional) whereas the Mg–B bonds are ionic (electrons more on the B side). For Zr the ionic effect is much lower, and there is a certain covalent bonding between Zr and B. The inplane conductivity is larger than the conductivity along z, but this anisotropy is larger for Mg than for Zr.

From these previous studies and our analysis it can be inferred that the boron layer is less likely to share electrons with the neighboring metal layer with respect to zirconium, that seems to have propensity to build a metallic interface in this case.

Whether or not this observation can be related to the larger work of adhesion in the latter system is matter for further and more accurate study (for example, with different mismatches and relative orientation of the two phases, and with a comparison with other metals like silver and copper).

5. Discussion

The unexpected spontaneous penetration of Au and Cu along the grain boundaries of ZrB_2 has been shown to take place after an incubation period during which a classical spreading kinetics takes place. Afterwards, the drop triple line does not move any more, and any contact angle decrease is due to volume shrinking. This effect should be linked to some "critical" value of the contact angle, connected to the geometry of voids and to the grain boundary energetics. For sure, the simultaneous interaction of the molten phase with the boride, as discussed in the following, can play an additional decisive role.

The initial evolution with time of contact angles, the absence of new interfacial phases and the data for enthalpy of mixing and surface tension derived from thermodynamic models, all suggest that the basic phenomena which govern the (Ag, Cu, Au)/ZrB_2 interactions are related to the dissolution of Zr into the molten metal. The liquid surface tension is affected also by Zr and B dissolution: however, while Zr is known to slightly increase the metal surface tension (at least in the low-concentration range) the boron effect has been calculated as significant but not larger than 10% in the range up to $X_B = 0.2$. This means that its effect on contact angles is small, if not negligible, and only after the contact angle has become less than 90°.

On the contrary, Zr can play a major role in promoting wetting. This has been shown several times[2,29] in brazing studies, where it has been used to promote wetting and adhesion in metal–ceramic systems.

The spontaneous dissolution of Zr into molten (Ag, Cu, Au) can be evaluated by the partial enthalpy of mixing at infinite dilution. These values, shown in Table 3 are in the same order of the work of adhesion. This supports the hypothesis that the "availability" of Zr, which increases in the order Ag < Cu < Au is the factor which determines the lowering of the equilibrium contact angle through Zr adsorption at the solid–liquid interface.

The calculations performed by the DFT technique give a strong support to this interpretation, clearly showing that, at the interface to the Zr-terminated ZrB_2 section, the metallic electronic distribution appears to penetrate down to the level of the zirconium layer, indicating the possibility of a metallic bonding at the interface. Moreover, they also are in agreement with an increasing work of adhesion in the order Ag < Cu < Au.

Finally, it is worth reminding that the term ($\gamma_{lv} \cos\theta$) represents the amount by which the solid surface tension is decreased by the solid–liquid interactions to give the interfacial tension value ($\gamma_{sv} - \gamma_{sl} = \gamma_{lv} \cos\theta$). Provided the solid surface tension does not vary in the present case, when going from one liquid metal to the other (indeed, similar metal matrix are used and the experimental conditions are the same), the values in the last column in Table 3 clearly show that Zr dissolved in Au is much more efficient in adsorbing/reacting at the interface and in promoting wetting.

6. Conclusions

A systematic study of the wettability of ZrB_2 by the metals Cu, Ag and Au has been made in order to find possible systematic interactions between the metal and the ceramic phases, without the presence of active additions or evident interfacial reactions.

It was found that Cu, Ag and Au behave in quite a different manner, from the completely non-wetting of silver to the good wetting of gold.

The presence of a nearly 10% open porosity in the sintered specimens gave the opportunity to show an unexpected result, i.e. the total penetration of gold and, to a lesser extent, of copper along the grain boundaries. This effect has been clearly evidenced by the simultaneous measurements of base diameters, height and contact angles of the various drops, as a function of time. Whether a specific contact angle, function of the porosity structure, exists, for which penetration takes place, is still a problem which deserves a dedicated exploration with ad hoc experiments.

However, the results obtained during the period where penetration does not macroscopilly appear, show that both Au and Cu should interact quite sensibly with the boride substrate, as shown by the steady variation of contact angle with time. This can only be due to dissolution of Zr and/or B into the molten metal. Boron can lower the liquid surface tension, as shown by ad hoc modelling, while Zr, whose dissolution enthalpy increases, in absolute value, in the order Ag < Cu < Au, entering the molten mass, can act as interfacially-active metal.

On the other hand, a common interesting feature, demonstrated by interfacial microstructures and EDS analysis, is that the metal–ceramic interface remains quite sharp after the wetting process, at variance with what happens with the same, or similar alloys with oxidic ceramics (e.g. alumina, zirconia[53–56]) thus allowing better mechanical properties to be obtained in the joining processes.

The conclusions reported in the previous lines are further supported by specific preliminary studies, by the DFT technique, on the projection of the density of states on localized orbitals at the interface. These calculations have shown an increase of the overlap between the density of states of Au and Zr at the Fermi energy, a signal in favour of the enhanced metallicity pertinent to this interface. A full account of this investigation will be given in a future publication.

Acknowledgements

The authors would like to express their appreciation to Dr. Alida Bellosi and Dr. Frederic Monteverde (ISTEC-CNR) for the preparation of ceramic samples and to Dr. Giorgio Battilana and Mr. Carlo Bottino (IENI-Ge) for SEM and EDS analyses.

References

1. Weimer, A. M., *Carbide Nitride and Boride Materials: Synthesis and Processing*. Chapman & Hall, New York, 1997.
2. Eustathopoulos, E., Nicholas, M. G. and Drevet, B., *Wettability at High Temperature*. Pergamon Materials Series, Elsevier Sci., Oxford, 1999.
3. Klein, R., Desmaison-Brut, M., Ginet, P., Bellosi, A. and Desmaison, J. J., *Eur. Ceram. Soc.*, 2005, **25**, 1757.
4. Nicholas, M. G., *Joining of Ceramics*. Chapman and Hall, London, 1990.
5. Espie, L., Drevet, B. and Eustathopoulos, N., *Metall. Trans.*, 1994, **25A**, 599.
6. Saiz, E. and Tomsia, A. P., *Nat. Mater.*, 2004, **3**, 903.
7. Gremillard, L., Saiz, E., Chevalier, J. and Tomsia, A. P., *Zeit Metallk Mater. Res. Adv. Tech.*, 2004, **95**, 261.
8. Saiz, E., Tomsia, A. P. and Saganuma, K., *J. Eur. Ceram. Soc.*, 2003, **23**, 2787.
9. Sciti, D., Melandri, C. and Bellosi, A., *Adv. Eng. Mater.*, 2004, **6**(9), 775.
10. Monteverde, F. and Bellosi, A., *J. Eur. Ceram. Soc.*, 2005, **25**, 1025.
11. Medri, V., Balbo, A., Monteverde, F. and Bellosi, A., *Adv. Eng. Mater.*, 2005, **7**(3), 159.
12. Monteverde, F. and Bellosi, A., *J. Mater. Res.*, 2004, **19**, 3576.
13. Monteverde, F. and Bellosi, A., *Adv. Eng. Mater.*, 2004, **6**, 33.
14. Monteverde, F. and Bellosi, A., *Adv. Eng. Mater.*, 2003, **5**, 508.
15. Monteverde, F., Bellosi, A. and Guicciardi, S., *Mat. Sci. Eng. A*, 2003, **346**, 310.
16. Eustathopoulos, N., Sobczak, N., Passerone, A. and Nogi, K., *J. Mater. Sci.*, 2005, **40**, 2271.
17. Saiz, E., Tomsia, A. P. and Cannon, R. M., *Scripta Mater.*, 2001, **44**, 159.
18. Arato, E., Costa, P. and Ricci, E., *J. Mater. Sci.*, 2005, **40**, 2133.
19. Ricci, E., Ratto, M., Arato, E., Costa, P. and Passerone, A., *ISIJ Int.*, 2000, **40**, 139.
20. Chatain, D., Ghetta, V. and Fouletier, J., In *Ceramic Microstructure: Control at the Atomic Level*, ed. A. P. Tomsia. Plenum, New York, 1998, p. 349.
21. Backhaus-Ricoult, M., *Acta Mater.*, 2000, **48**, 4365.
22. Laurent, V., Chatain, D. and Eustathopoulos, N., *Acta Met.*, 1988, **36**, 1797.
23. Castello, P., Ricci, E., Passerone, A. and Costa, P., *J. Mater. Sci.*, 1994, **29**, 6104.
24. Ratto, M., Ricci, E. and Arato, E., *J. Cryst. Growth*, 2000, **217**, 233.
25. Kotsch, H., *Neue Hütte*, 1967, **12**, 350.
26. Ukov, V. P., Esin, O. A., Vatolin, N. A. and Dubinin, E. L., *Physical Chemistry of Interfacial Phenomena at High Temperature*. Kiev, Naukova Dumka, 1971, p. 139.
27. Samsonov, G. V., Panasyuk, A. D. and Borovikova, M. S., *Poroshkovaya Metall.*, 1973, **5**, 61.
28. Passerone, A. and Ricci, E., *Drops and Bubbles in Interfacial Research*, *Vol. 6*, ed. D. Moebius and R. Miller. Elsevier, Amsterdam, 1998, p. 475.
29. Muolo, M. L., Ferrera, E., Novakovic, R. and Passerone, A., *Scripta Mater.*, 2003, **48**, 191.
30. Liggieri, L. and Passerone, A., *High Temp. Techn.*, 1989, **7**, 80.
31. Viviani, M., Liggieri, L. and Passerone, A., *IENI-CNR Technical Report*, CNR Genoa, 2002.
32. Massalski, T. B., *Binary Alloy Phase Diagrams*, *Vol. 1*. Am Soc for Metals, Ohio, 1986, p. 235 and 350.
33. Tanaka, T., Gocken, N. A., Morita, Z.-I. and Iida, T., *Z. Metallkd.*, 1993, **84**, 192.
34. Witusiewicz, V. T., *J. Alloys Compd.*, 1995, **221**, 74.
35. Singh, R. N., *Can. J. Phys.*, 1987, **65**, 309.
36. Anusionwu, B. C. and Adebayo, G. A., *J. Alloys Compd.*, 2001, **329**, 162.
37. Millot, F., Rifflet, J. C., Sarou-Kanian, V. and Wille, G., *Int. J. Thermophys.*, 2002, **23**(5), 1185.
38. Fitzner, K. and Kleppa, O. J., *Metall. Trans.*, 1992, **A23**, 997.
39. Lomello-Tafin, M., Galez, P., Feschotte, P., Kuntz, J. J., Jorda, J. L. and Gachon, J. C., *J. Alloys Compd.*, 1998, **267**, 142.
40. Kleppa, O. J. and Watanabe, S., *Metall. Trans. B*, 1982, **13B**, 391.
41. Witusiewicz, V., Arpshofen, I. and Sommer, F., *Z. Metallkd.*, 1997, **88**(11), 866.
42. Sommer, F. and Choi, D. K., *Z. Metallkd.*, 1989, **80**(4), 263.
43. Zaitsev, A. I., Zaitseva, N. E., Alekseeva YuP, Kuril'chenko, E. M. and Dunaev, S. F., *Inorg. Mater.*, 2003, **39**(8), 816.
44. Novakovic, R., Muolo, M. L. and Passerone, A., *Surf. Sci.*, 2004, **549**, 281.
45. Novakovic, R., Tanaka, T., Muolo, M. L., Lee, J. and Passerone, A., *Surf. Sci.*, 2004, **591**, 56.
46. Vozdvizhenski, V. M., *Prognoz dvoinih diagram sostoyaniya po statistich-eskim kriteriyam*. Metallurgiya, Moskva, 1975.
47. Finnis, M. W., *J. Phys.-Condensed Matter*, 1996, **8**, 5811.
48. Baroni, S., Dal Corso, A., De Gironcoli, S., Giannozzi, P., Cavazzoni, C., Ballabio, G., Scandolo, S., Chiarotti, G., Focher, P., Pasquarello, A., Laasonen, K., Trave, A., Car, R., Marzari, N. and Kokalj, A., http://www.pwscf.org/.
49. Dudyi, S. V. and Lundqvist, B., *Phys. Rev. B*, 2004, **69**, 125421.
50. Shishidou, T. *et al.*, *J. Appl. Phys.*, 2003, **93**, 6876.
51. de la Mora, P., Castro, M. and Tavizon, G., *J. Solid State Chem.*, 2002, **169**, 168.
52. Bakker, H., *Enthalpies in Alloys—Miedema's Semi-Empirical Model*. Trans Tech Publ. Ltd., Switzerland, 1998.
53. Kritsalis, P., Coudurier, L. and Eustathopoulos, N., *J. Mater. Sci.*, 1991, **26**, 3400.
54. Iwamoto, N. and Yokoo, H., *J. Mater. Sci.*, 1992, **27**, 441.
55. Torvund, T., Grong, Ø., Akselsen, O. M. and Ulvensoen, J. H., *Metall. Mater. Trans. A*, 1996, **27A**, 3630.
56. Sciti, D., Bellosi, A. and Esposito, L., *J. Eur. Ceram. Soc.*, 2001, **2**, 45.